MPPT algorithm based on modified remora optimization algorithm for photovoltaic systems under partial shading conditions

Moh. Zaenal Efendi [a], Akhmad Adnaurrosyid [a, *], Muhammad Nizar Habibi [a],
Rachma Prilian Eviningsih [a], Novie Ayub Windarko [a], Mentari Putri Jati [b]

[a] Electrical Engineering Department, Politeknik Elektronika Negeri Surabaya
Jalan Raya ITS Sukolilo Kampus PENS, Surabaya, 60111, Indonesia

[b] National Taipei University of Technology
No.1, Section 3, Zhongxiao East Road, Taipei, 10608, Taiwan

Abstract

The increasing electricity demand, driven by the growing human population, has led to the need for efficient backup power sources. Solar panels are one of the renewable energy sources that have been widely developed because they only require solar energy as their primary source. However, the phenomenon of partial shading is often a problem in solar panels because it can reduce the output power of the solar panel system, which is caused by shadows from trees or clouds. In this condition, conventional maximum power point tracking (MPPT) algorithms are often limited to the local maximum power point (LMPP). To effectively attain the global maximum power point (GMPP), it is imperative to devise more efficient algorithms. The modified remora optimization algorithm (MROA) has been proposed as a potential solution to this challenge. MROA is an adaptation of the remora optimization algorithm (ROA), inspired by the behavior of remora fish. The results indicate that the algorithm achieves an average accuracy of approximately 99.13 % in both simulation and hardware implementations. Furthermore, when comparing the results of the MROA with those of the original ROA method and particle swarm optimization (PSO), the MROA exhibited superior accuracy, tracking time, and power gain, suggesting that the MROA algorithm effectively circumvents the limitation of the local maximum power point.

Keywords: solar panel; partial shading; maximum power point tracking (MPPT); modified remora optimization algorithm (MROA).

I. Introduction

With the advancement of industrial automation, digitalization, and the widespread adoption of smart devices and communication systems, there has been a concomitant increase in the global demand for electrical energy [1]. This increasing dependence on electricity necessitates the development of energy-efficient, clean, and reliable power sources, particularly in regions with unstable grid access or variable load demands [2]. Among the various renewable energy options, solar energy is particularly promising because of its sustainability, abundance, and environmental friendliness [3][4].

Photovoltaic (PV) systems are extensively used to capture solar energy by directly converting sunlight into electrical energy [5]. These systems offer

How to Cite: M. Z. Efendi *et al.*, "MPPT algorithm based on modified remora optimization algorithm for photovoltaic systems under partial shading conditions," *Journal of Mechatronics, Electrical Power, and Vehicular Technology*, vol. 16, no. 2, pp. 204-219, Dec., 2025.

advantages such as minimal maintenance requirements, scalability, and silent operation. However, their efficiency is significantly affected by environmental factors, particularly partial shading conditions (PSC) [6][7]. PSC occurs when sections of a PV array are obscured by objects such as clouds, trees, or buildings, leading to uneven current production and altered power-voltage (P–V) characteristics [8][9]. This alteration results in the formation of multiple local maximum power points (LMPP), which can impede the system from reaching the global maximum power point (GMPP), thereby causing substantial power losses [10].

To address this issue, maximum power point tracking (MPPT) algorithms are integrated into photovoltaic (PV) systems to ensure continuous and optimal energy extraction. Traditional MPPT techniques, such as perturb and observe (P&O), incremental conductance (INC), and hill climbing (HC), are extensively employed because of their ease of implementation and minimal computational requirements [11][12]. However, their efficacy is reduced under partial shading conditions (PSC) because of their limited tracking capabilities and propensity to become trapped at the local maximum power point (LMPP) [13][14]. Attempts to improve their performance using adaptive step sizes and modified control rules have yielded only partial success [15][16].

In response to the limitations inherent in traditional maximum power point tracking (MPPT) methods, numerous researchers have explored intelligent optimization techniques, particularly metaheuristic algorithms, which are adept at performing global searches within complex, nonlinear, and multi-modal problem environments [17][18]. Initially, particle swarm optimisation (PSO) was employed for maximum power point tracking (MPPT) and became widely favored due to its straightforwardness and quick convergence. However, PSO often faces challenges with early convergence, particularly in situations with fluctuating radiation levels [19]. Similarly, genetic algorithms (GA) exhibit robust global exploration capabilities but encounter difficulties in adjusting crossover and mutation rates, leading to significant processing delays [20].

Alternative nature-inspired methodologies, such as grey wolf optimization (GWO), ant colony optimization (ACO), and artificial bee colony (ABC), have been explored for maximum power point tracking (MPPT) applications. The GWO simulates the hunting strategies of wolf packs but may encounter difficulties with convergence precision [21]. Although ACO and ABC are generally more exploratory, they face

challenges related to increased computational demands and unstable tracking during rapid shading variations [22][23]. Recent strategies, including the reptile search algorithm (RSA) [24], falcon optimization algorithm (FOA) [25], and tunicate swarm algorithm (TSA) [26], have been developed to improve global optimization under partial shading conditions (PSC). Nonetheless, these approaches also exhibit limitations, such as steady-state oscillations, sensitivity to initial conditions, and extended convergence times, which constrain their efficacy for real-time MPPT.

To address these challenges, algorithms inspired by marine organisms have been developed. A prominent example is the remora optimization algorithm (ROA), which mimics the behavior of remora fish that attach themselves to larger marine animals to improve their navigation and foraging strategies. ROA presents a promising balance between exploration and exploitation through dynamics similar to a shoal and the cooperative movement of agents. However, ROA still faces difficulties such as population stagnation, insufficient adaptive search control, and reduced tracking performance in dynamic environments [27].

To tackle these shortcomings, the modified remora optimization algorithm (MROA) was formulated as an enhanced variant of ROA. The MROA integrates advanced position-update strategies, adaptive learning components, and dynamic search agents to enhance responsiveness and tracking precision. In contrast to earlier iterations, the MROA was optimized for real-time applications by minimizing oscillations and improving convergence reliability. This algorithm is specifically designed to overcome the deficiencies of previous models and facilitate the development of high-performance, low-complexity maximum power point tracking (MPPT) controllers for photovoltaic (PV) systems affected by partial shading.

This study investigates the application of the MROA for MPPT in PV systems under PSC, situating the algorithm within the context of extensive prior research. By addressing the limitations inherent in both traditional and intelligent MPPT methods, MROA offers an alternative approach that integrates biological intelligence and algorithmic enhancement.

II. Materials and Methods

A. Design MPPT system

MPPT systems require a voltage control circuit to function optimally; therefore, a buck-boost converter is needed to adjust the voltage obtained from the PV to match the load demand. This converter was selected based on its ability to self-adjust the voltage according
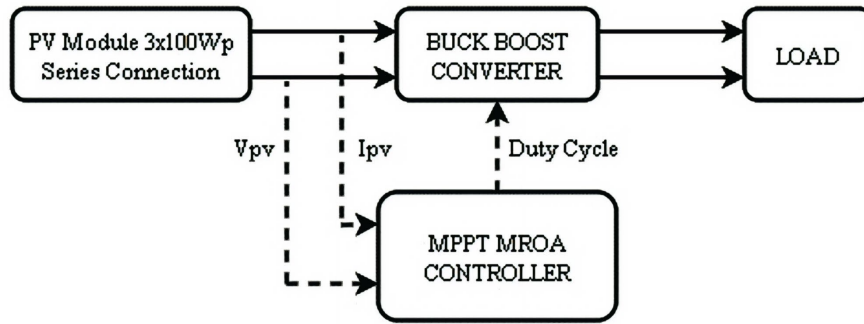
Figure 1. Diagram block MPPT system.

to the system conditions. A block diagram of the MPPT system is shown in Figure 1.

B. Photovoltaic system

Photovoltaic (PV) systems convert sunlight into electricity through the photovoltaic effect, wherein photons excite electrons within a semiconductor, typically silicon, resulting in the production of a direct current (DC). The efficiency of this process depends on the type of semiconductor, system design, and the intensity of sunlight. The current-voltage (I-V) characteristics of the PV panel are represented in equation (1), whereas the photovoltaic current I_{ph}, generated as a result of solar irradiance, is described in equation (2) [28].

$$I = I_{ph} - I_0 \left(e^{\frac{q(V-IR_S)}{nkT}} - 1 \right) - \frac{V+IR_S}{R_{sh}} \qquad (1)$$

$$I_{ph} = \left[I_{sc} + \alpha\left(T - T_{ref}\right) \right] \frac{G}{G_{ref}} \qquad (2)$$

where I is the output current (A) and V is the output voltage (V) at the terminal connected directly to the load. I_0 is the diode saturation current (A), I_{ph} is the photovoltaic current generated by solar irradiance (A), R_S and R_{sh} are the series and shunt (parallel) resistances of the PV panel (Ω), respectively. q is the electron charge (1.6×10^{-19} C), k is Boltzmann's constant ($1.3806503 \times 10^{-23}$ J/K), and n is the ideality factor of the diode (dimensionless). Then, in equation (2), I_{sc} is the short-circuit current of the PV panel (A) under standard test conditions (STC), G is the solar irradiance received by the PV panel (W/m^2),

and G_{ref} is the reference irradiance in STC (1000 W/m²). T is the cell temperature (K), and T_{ref} is the reference temperature in STC (298.15 K). The parameter α represents the temperature coefficient of short-circuit current (A/K). PV panels used for this system are Solana Monocrystalline 100 Wp. Figure 2 shows the electrical equivalent circuit of a solar cell.

The specifications of the solar panels were customized to align with the system design for optimal power output. Table 1 presents the specifications of the solar panels.

C. Partial shading condition (PSC)

Partial shading occurs when a portion of a solar panel is obscured by nearby objects, such as tree shadows, buildings, or other barriers. This condition results in the formation of multiple power peaks, referred to as maximum power points (MPP). The number and values of these MPPs are influenced by the configuration of the photovoltaic (PV) array and the extent of shading. Under partial shading conditions, the characteristic curve of the PV array exhibits multiple power peaks. The highest of these peaks is identified as the global maximum power point (GMPP), whereas the smaller peaks are termed local maximum power points (LMPP) [29]. As the shading effect intensified, additional LMPPs emerged, leading to a significant reduction in the total power output of the solar panel. Partial shading reduces the efficiency of
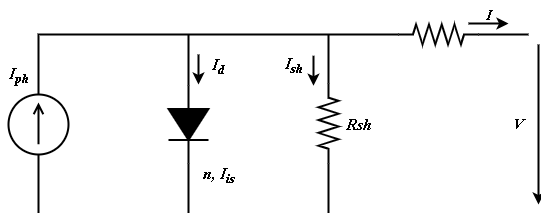

Figure 2. Electrical equivalent circuit of a solar cell.

Table 1.
PV module specification.

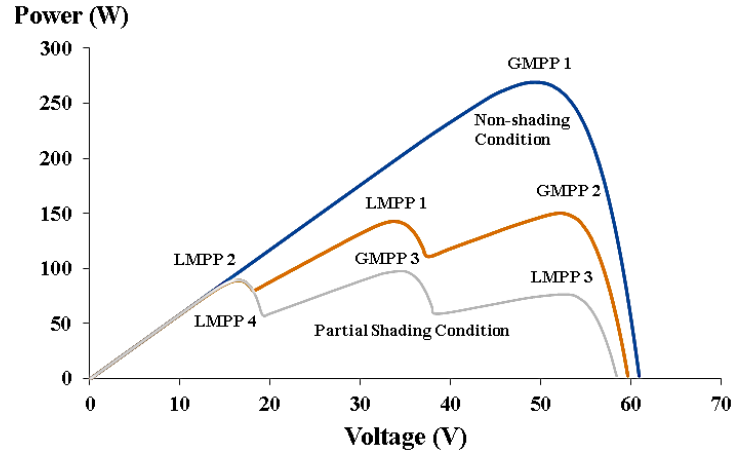| Parameter	Value
Max. power (P_{max})	100 Wp
Open-circuit voltage (V_{oc})	22.1V
Short-circuit current (I_{sc})	5.81A
Optimum operating voltage (V_{mp})	18.3V
Optimum operating current (I_{mp})	5.47A
Dimension	800×670×30mm
Test condition	1000 W/m^2, 25°C

Figure 3. PV characteristics.

solar panels because not all sections of the panel receive a uniform light intensity. Consequently, some cells produce less power, thereby affecting the overall system output. There is an inverse correlation between partial shading and the power output of solar panels. The more pronounced the partial shading, the lower the maximum power generated by the panels [30]. This is because photovoltaic systems rely on solar irradiance to generate electrical power. Figure 3 illustrates the PV characteristic curve.

D. DC-DC buck boost converter

A DC–DC buck–boost converter is designed to regulate the output voltage to be either higher or lower than the input voltage, depending on the system requirements. This study models the converter by incorporating the nonlinear behavior of the inductor, particularly under conditions of magnetic saturation, which influences energy transfer and system performance. The converter comprises a MOSFET switch, a nonlinear inductor with current-dependent inductance, a diode for discharge during the off-state, a capacitor to smooth the output voltage, and a resistive load. Nonlinear effects, such as variable inductance and core losses, are necessary to generate an accurate model. The model also accounts for electrical losses arising from conduction, switching, and the magnetic core, all of which affect the efficiency and dynamics of the converter [31]. The parameter of the boost converter is obtained from equation (3) to equation (6).

$$V_o = -V_s \left(\frac{D}{1-D} \right) \tag{3}$$

$$D = \frac{|V_o|}{V_s + |V_o|} \tag{4}$$

$$L = \frac{(1-D)^2 R}{2f} \tag{5}$$

$$C = \frac{V_o D}{\Delta V_o R f} \tag{6}$$

In the equations of the buck-boost converter, V_o denotes the output voltage of the converter, measured in volts, whereas V_s represents the input voltage, which is also expressed in volts. The variable D signifies the duty cycle, which is the ratio of the ON time of the switch to the total duration of the switching cycle and is dimensionless. The inductance is indicated by L and is quantified in henries (H), whereas R represents the load resistance, measured in ohms (Ω). The switching frequency is denoted by f and measured in hertz (Hz). Capacitance is represented by C and is expressed in farads (F), and ΔV_o refers to the allowable ripple voltage at the output, measured in volts. Figure 4 presents a schematic representation of the buck–boost converter. Table 2 summarises the parameter values pertinent to the boost converter.

E. Modified remora optimization algorithm

The remora optimization algorithm (ROA) draws inspiration from the natural behaviour of remora fish, which attach themselves to larger marine animals, such as fish or whales, to enhance their ability to locate food.

Table 2.
Component value of the buck-boost converter

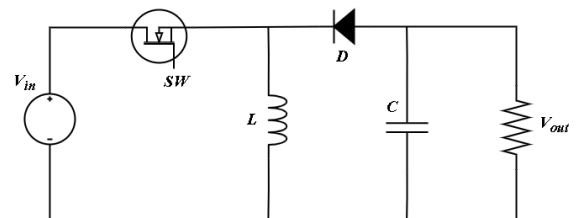| Parameter	Value
Capacitor (C)	2200 µF
Inductor (L)	251µH
Resistor load (R)	3Ω
Switching frequency (f)	40kHz

Figure 4. Buck boost converter circuit.

This concept is incorporated into the optimization process through a movement scheme for solution agents that mimics the attachment and movement relative to the host position. Within this algorithm, the exploration and exploitation phases are structured using parameters that regulate the intensity of movement toward the optimal solution. ROA demonstrates its capability to perform an effective global search while ensuring stable convergence, rendering it suitable for application in various nonlinear and multipeak optimization challenges without necessitating the integration of strategies from other algorithms [32].

1) Exploration

The remora optimization algorithm (ROA) utilizes the Swordfish optimization (SFO) strategy to conduct an exhaustive global search by leveraging the advanced methodology of the swordfish algorithm. The formula for updating the position is expressed by equation (7).

$$V_i(t+1) = X_{best}(t) - \left(rand \times \left(\frac{X_{best}(t) + X_{rand}(t)}{2} \right) - X_{rand}(t) \right) \tag{7}$$

Where $V_i(t+1)$ represents the updated position of the i_{th} remora, $X_{best}(t)$ denotes the current optimal position, $X_{rand}(t)$ is the random position of a remora, t is the current iteration number, and $rand$ is a random value between 0 and 1. In addition, the remora may change hosts based on previous experience. In such instances, a new candidate position can be determined using the following equation (8).

$$V_i'^{(t+1)} = V_i(t+1) + rand \times (V_i(t+1) - X_i(t)) \tag{8}$$

where $V_i'^{(t+1)}$ is the new candidate position of the i_{th} remora, $X_i(t)$ is the previous position, and $rand$ generates a normally distributed random number.

2) Exploitation

Remoras possess the ability to attach themselves to humpback whales, thereby gaining access to food sources. As a result, remoras have adopted the movement patterns of these whales. In the remora optimization algorithm (ROA), the strategy derived from the whale optimization algorithm (WOA) is used to enhance local search capabilities. ROA incorporates the bubble-net hunting method employed in WOA. The formula for updating the position is expressed by equation (9):

$$V_i(t+1) = D \times e^a \times cos(2\pi a) + X_{best}(t) \tag{9}$$

$$D = |X_{best}(t) - X_i(t)| \tag{10}$$

$$\alpha = rand \times (b-1) + 1 \tag{11}$$

$$b = -\left(1 + \frac{t}{T}\right) \tag{12}$$

In this context, D represents the distance between the remora and the food source. According to equation (11) and equation (12), α is a random variable ranging from −2 to 1, whereas b decreases linearly from −1 to −2.

Furthermore, to enhance the quality of the solution, remoras can implement minor adjustments utilizing the prey encircling mechanism from the whale optimization algorithm (WOA), which is defined by equation (13).

$$X_i(t+1) = V_i(t+1) + A \times D' \tag{13}$$

$$A = 2 \times B \times rand - B \tag{14}$$

$$B = 2 \times \left(1 - \frac{t}{T}\right) \tag{15}$$

$$D' = V_i(t+1) - C \times X_{best}(t) \tag{16}$$

where $X_i(t+1)$ indicates the updated position of the ith remora, and C represents the remora factor, set to 0.1 in the remora optimization algorithm (ROA).

The proposed modification of the autonomous foraging mechanism (AFM) introduces two distinct operators to optimize the performance of the remora optimization algorithm (ROA) [33]. Initially, the remora possesses a small probability, denoted by x, to explore a novel, uncharted location for sustenance. If $rand < x$ is met, the remora will undertake a comprehensive and random search across the entire area. The corresponding mathematical expression is presented in equation (17).

$$X_i(t+1) = (UB - LB) \times rand + LB \tag{17}$$

where UB and LB denote the upper and lower bounds of the search space, respectively.

As demonstrated by equation (17), the initial operator enhances the exploration capability of ROA, thereby effectively preventing it from becoming ensnared at a local optimum. Conversely, to augment the exploitation capability of ROA, the position update equation is as follows equation (18) and equation (19).

$$X_i(t+1) = \begin{cases} X_{best}(t) : (RMOP + eps) \times \left((UB - LB) \times \mu + LB\right) \\ \qquad \times Levy, rand < 0.5 \\ X_{best}(t) \times RMOP \times \left((UB - LB) \times \mu + LB\right) \times \\ \qquad Levy, rand \geq 0.5 \end{cases} \tag{18}$$

$$RMOP = 1 - \left(\frac{t}{T}\right)^{1/\alpha} \tag{19}$$

$$\alpha = 10 \times rand - 1 \tag{20}$$

The random math optimizer probability (RMOP) is computed using the current iteration number, the total possible iterations, and the parameter $\propto$. As defined in equation (20), $\propto$ is a random number that can range from −1 to 9. According to equation (12), the updated position is determined based on the current optimal position, which signifies the food source. Additionally, the *Levy* operator is employed to enhance the diversity of the population. A flowchart representation of the MROA in MPPT is shown in Figure 5.

The MROA search strategy is excellent at quickly finding the convergence points to identify GMPPs. As shown in Figure 5, the MROA starts by setting up the initial state, the remora position, the duty cycle

distribution, the maximum iteration, and the number of agents. Then, it arranges the initial remora positions based on their best power. In each loop, the remora positions are updated using their hunting method based on equation (17), equation (18), and equation (13). Random values determine the exploitation phase. When the value is less than z, equation (17) should be employed; if it is less than y, then equation (18) should be applied. In the absence of these conditions, equation (13) should be used. The solutions help to find the best power value recalculated in each loop. The optimal remora position for finding food is the best solution. All MROA steps, except for the start and sensor readings, were repeated until the
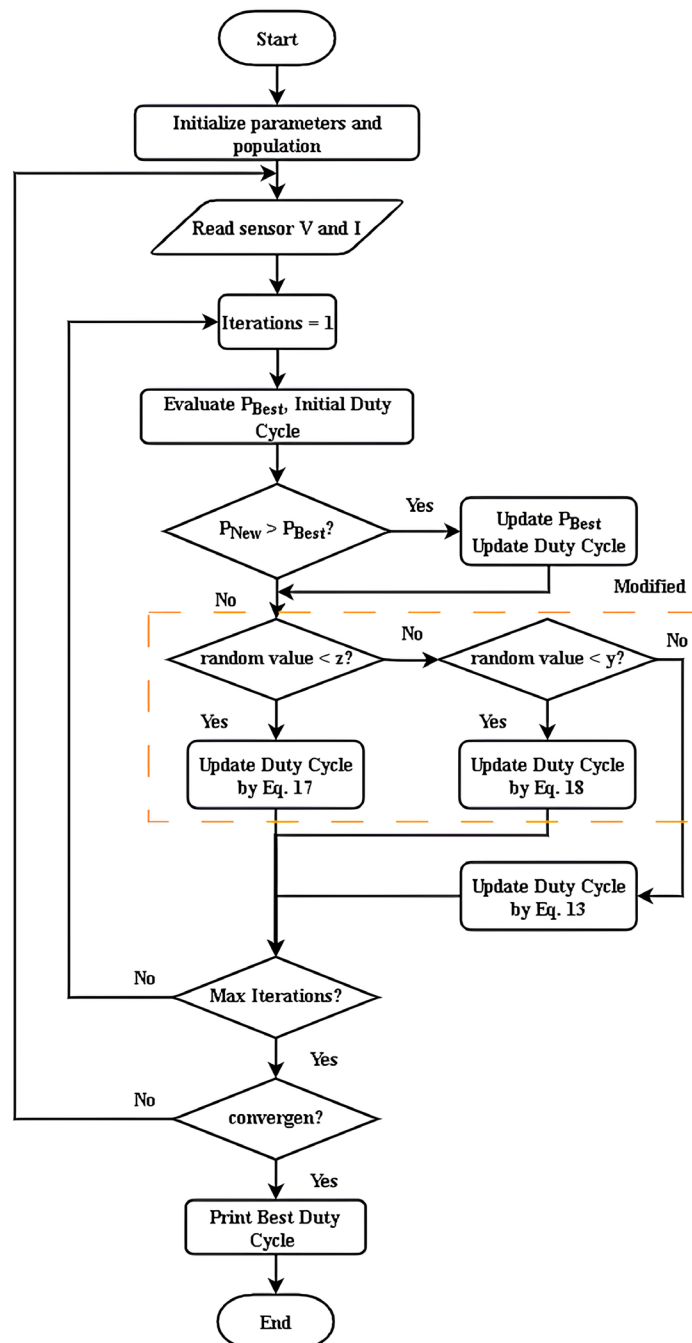

Figure 5. Flowchart of modified remora optimization algorithm (MROA) for MPPT.
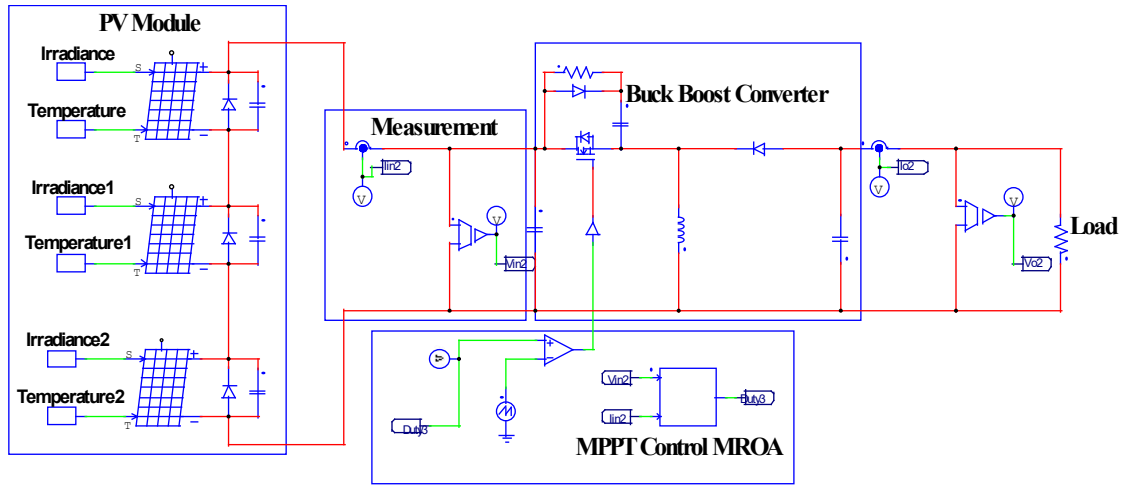
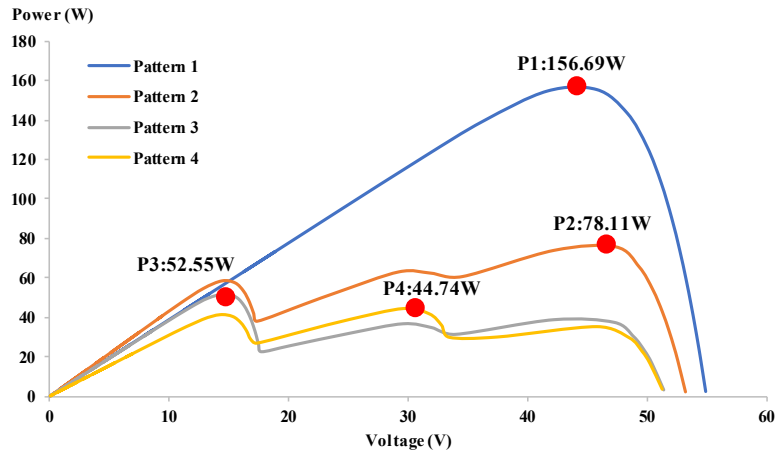Figure 6. Proposed MPPT control simulation model.

Figure 7. P-V characteristics of the simulated test pattern.

maximum iterations had been reached. As an MPPT controller, the MROA should be able to quickly reach the GMPP condition with little oscillation, thereby improving the system performance.

III. Results and Discussions

A. Simulation test

This section presents an analysis of a photovoltaic (PV) system with Maximum Power Point Tracking (MPPT) implemented in PSIM. As illustrated in Figure 6, the system consists of three PV panels connected in series, a buck-boost converter, an MPPT controller, and a resistive load. The MPPT controller, tasked with identifying the maximum power point (MPP) under varying irradiation and shading conditions, was assessed using the modified remora optimization algorithm (MROA) and compared to the original ROA and particle swarm optimization (PSO). The results demonstrate that MROA outperforms both alternatives in terms of tracking speed, stability, and accuracy, which is attributed to its robust global search

capability and resistance to local optima in partial shading scenarios. Table 3 delineates the parameter configuration of the algorithm. Several strategies were implemented to ensure an equitable testing process.

The experiment utilised six particles and was conducted up to ten times. All the agents were initialized with identical values. The efficacy of the proposed MROA was evaluated under two conditions: without shading and with partial shading. Table 4 lists the various configurations of the PV system, achieved by adjusting the light and temperature to align with the actual equipment. Figure 7 illustrates the power-voltage (P-V) characteristics of these configurations. Pattern 1

Table 3.
Specification of parameters used in the algorithm.

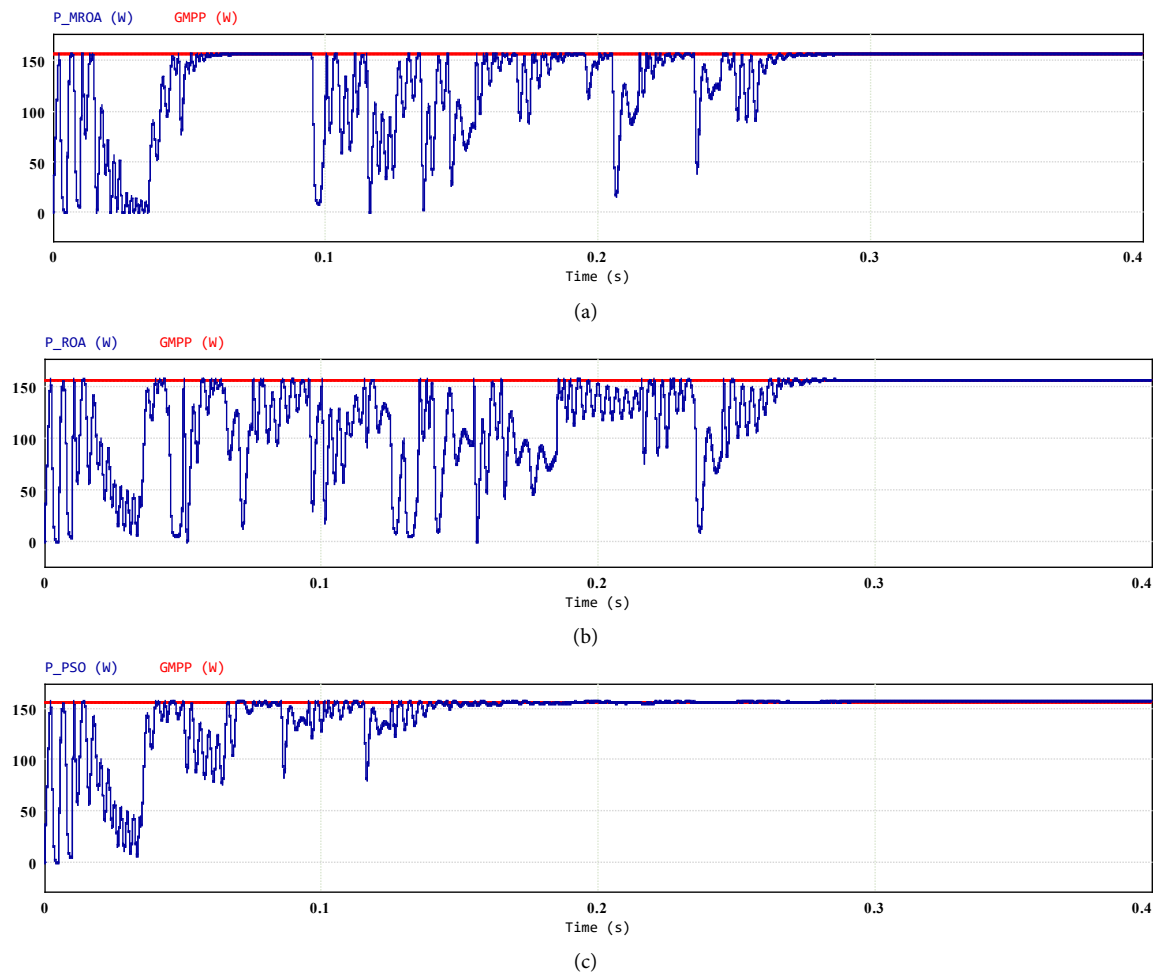| Algorithm	Parameter
MROA	$C = 0.1; \alpha\epsilon[-1,9]; \mu = 0.499; z = 0.07; y = 0.1$
ROA	$C = 0.1$
PSO	$C1 = 0.8; C2 = 0.8$

Figure 8. The simulation results of the algorithms pattern 1: (a) MROA; (b) ROA; and (c) PSO.

corresponds to the condition without shading, characterized by a single main power point with a peak power of 156.69 W. Patterns 2, 3, and 4 represent conditions with partial shading, resulting in multiple smaller power points along one primary peak. These conditions stem from the arrangement of the three PV panels connected in series. The main power point in PATTERN 2 was 78.11 W, in PATTERN 3 was 52.55 W, and in PATTERN 4 was 44.74 W.

Figure 8 presents the tracking performance of MROA, ROA, and PSO under Pattern 1 with a GMPP of 156.69 W. MROA achieved the highest efficiency, reaching 156.67 W (99.99 %) within 0.276 s. ROA followed with 156.58 W (99.93 %) in 0.284 s, while PSO

produced 156.21 W (99.69 %) in 0.285 s. These results confirm MROA's superiority in both tracking speed and accuracy.

Figure 9 illustrates the power-tracking response for MROA, ROA, and PSO under Pattern 2. The GMPP is 78.11 W, with MROA achieving 78.09 W, reflecting an accuracy of 99.97 % within 0.294 s. Both ROA and PSO attained 78.04 W, corresponding to an accuracy of 99.91 % in 0.295 s. Consequently, the MROA exhibits superior precision and expedited tracking performance in this context.

Figure 10 illustrates the power tracking capability of the MROA, ROA, and PSO on PATTERN 3, where it closely approximates the GMPP of 52.55 W by

Table 4.
Solar irradiance patterns under various conditions.

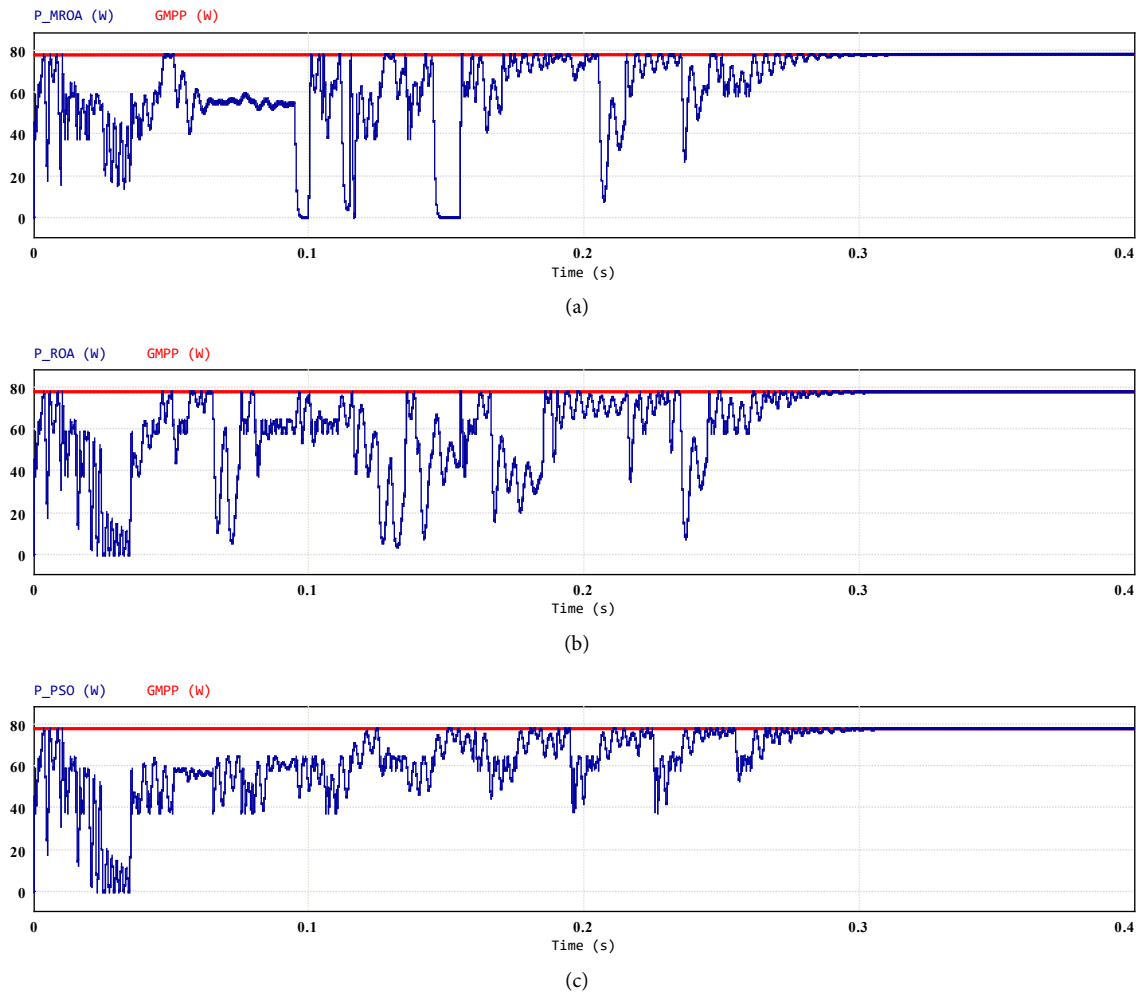| Pattern	Irradiance			GMPP
	PV 1 (W/m^2)	PV 2 (W/m^2)	PV 3 (W/m^2)	
1	1000	1000	1000	156.69 W
2	1000	750	500	78.11 W
3	250	1000	500	52.55 W
4	500	667	1000	44.74 W

Figure 9. The simulation results of the algorithms pattern 2: (a) MROA; (b) ROA; and (c) PSO.

achieving an output power of 52.30 W, with an accuracy of 99.52 % and a tracking duration of 0.268 s. The ROA algorithm required 0.271 s to generate 52.27 W of power with 99.47 % accuracy, slightly lagging behind MROA in terms of speed and precision. PSO, which is the fastest method with a tracking time of 0.220 s, produces 52.2 W of power with 99.33 % accuracy. These findings suggest that in this pattern, MROA excels in terms of accuracy, whereas PSO provides the advantage of the fastest tracking time.

Figure 11 depicts the results of GMPP tracking using the MROA, ROA, and PSO algorithms in Pattern 4. The GMPP value is 44.74 W, with MROA achieving a power output of 44.63 W, an accuracy of 99.75 %, and a tracking time of 0.270 s. The power tracking of the ROA algorithm requires 0.272 s, which is able to produce 44.58 W of power, with 99.64 % accuracy, which is marginally lower than that of MROA. The performance of the PSO algorithm was notably lower, yielding a power output of merely 41.45 W, with an accuracy rate of 92.65 %, and a tracking time of 0.287 s. In this complex shading pattern, MROA proves to be more reliable and significantly outperforms both ROA and PSO in accuracy and power output.

Figure 8 to Figure 11 depict the performance of the MROA, ROA, and PSO algorithms under partial-shading conditions. Although all three algorithms are capable of identifying the global maximum power point (GMPP), they exhibit variations in accuracy, response time, and power stability. The PSO algorithm demonstrated the fastest response time (approximately 0.271 s) but lacked stability, particularly in Pattern 4, with an average accuracy of 97.89 %. The ROA algorithm offers enhanced stability and higher accuracy (99.73 %), but operates at a slightly slower pace (approximately 0.28 s). The MROA algorithm surpasses both, achieving an accuracy of 99.81 %, rapid tracking time (approximately 0.277 s), and robust post-GMPP power stability, thereby optimizing the energy harvesting. Due to its balanced performance in terms of speed, accuracy, and stability, the MROA algorithm emerges as the most reliable maximum power point tracking (MPPT) method among the three for managing varying shading patterns in photovoltaic (PV) systems. Table 5 presents a detailed overview of the simulation results.
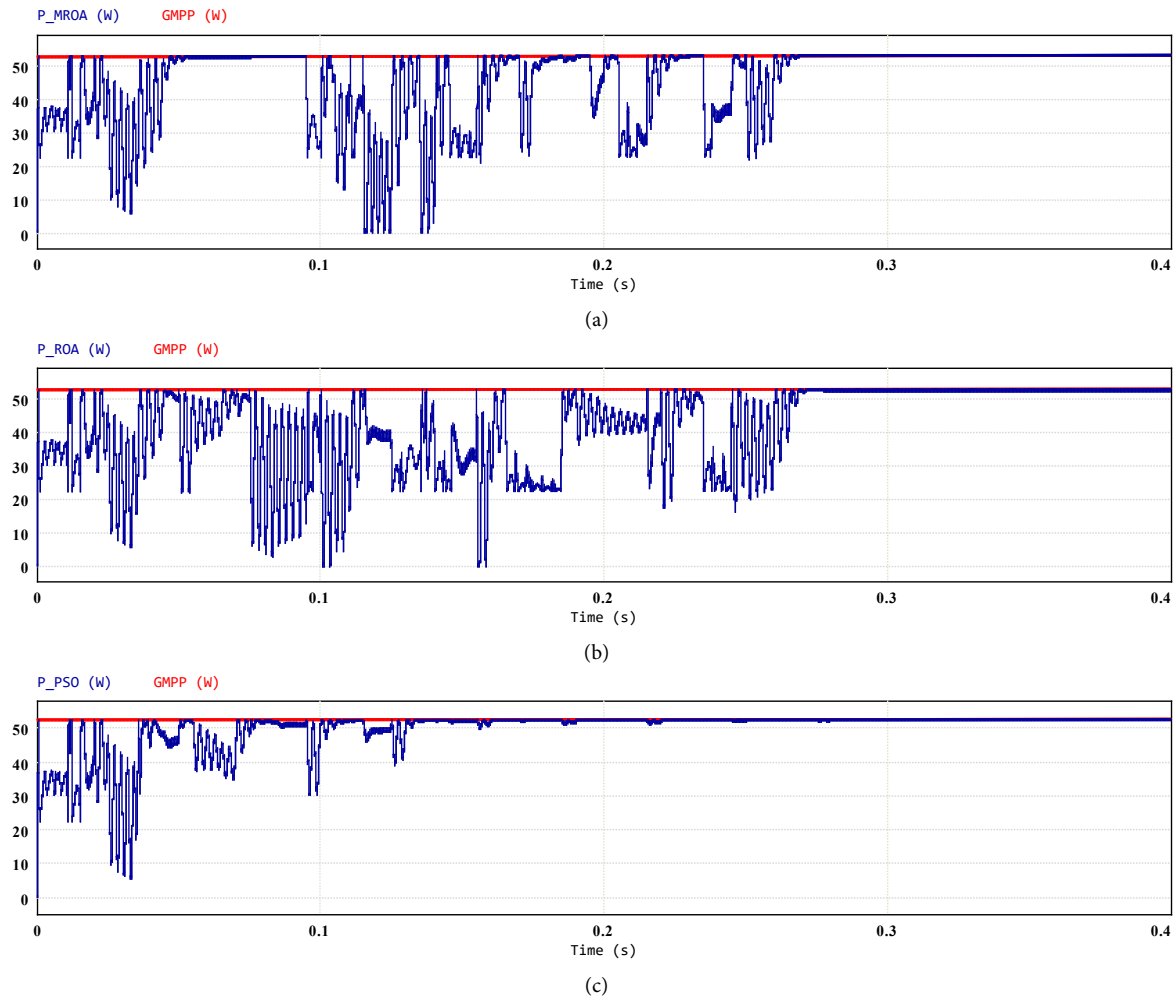
Figure 10. The simulation results of the algorithms pattern 3: (a) MROA; (b) ROA; and (c) PSO.

B. Experimental test

Figure 12 illustrates the experimental setup, comprising a set of three 100 Wp solar panels connected in series, a buck-boost converter, voltage and current sensors, an STM32 microcontroller for MPPT control, and a fixed resistor load. Testing was conducted under natural sunlight with panels positioned at an optimal angle to capture direct irradiance, which varied between 800 and 1100 W/m². The panel output was continuously monitored and logged using telemetry software interfaced with a microcontroller. The MPPT tracking employed the MROA, ROA, and PSO algorithms sequentially to

Table 5.
Simulation results data.

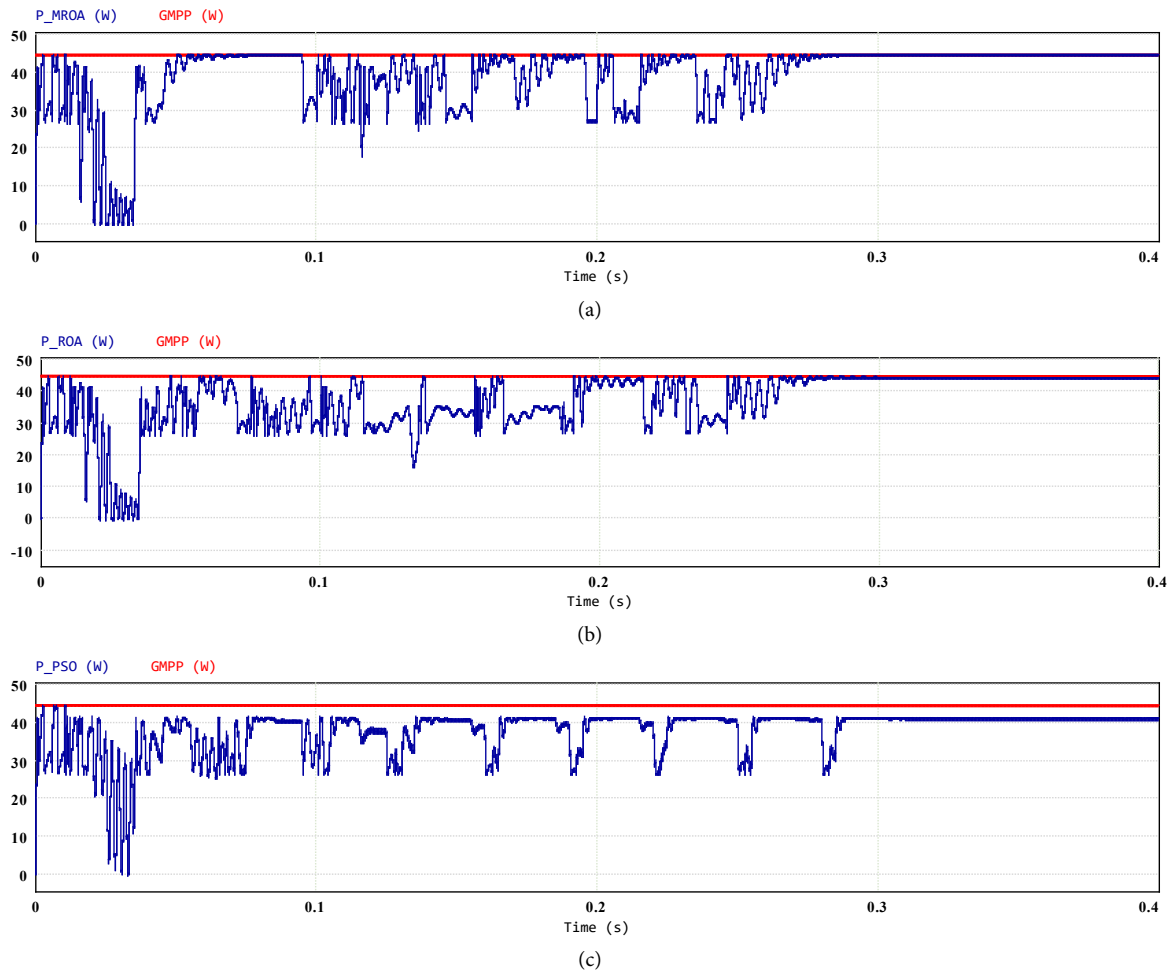| Pattern	Algorithm	GMPP (W)	Power output (W)	Accuracy (%)	Time tracking (s)
1	MROA	156.69	156.67	99.99	0.276
	ROA	156.69	156.58	99.93	0.284
	PSO	156.69	156.21	99.69	0.285
2	MROA	78.11	78.09	99.97	0.294
	ROA	78.11	78.04	99.91	0.295
	PSO	78.11	78.04	99.91	0.295
3	MROA	52.55	52.30	99.52	0.268
	ROA	52.55	52.27	99.47	0.271
	PSO	52.55	52.20	99.33	0.220
4	MROA	44.74	44.63	99.75	0.270
	ROA	44.74	44.58	99.64	0.272
	PSO	44.74	41.45	92.65	0.287

(a)

(b)

(c)

Figure 11. The simulation results of the algorithms pattern 4: (a) MROA; (b) ROA; and (c) PSO.

evaluate their performance under identical real-world conditions. The evaluation metrics include the maximum power output, tracking stability, and convergence speed of the GMPP. Figure 13 presents the resulting P–V characteristics, which reflect the dynamic power response during tracking. The incorporation of natural sunlight enhances the reliability of performance evaluation in realistic contexts.

In Pattern 1, the global maximum power point (GMPP) was 154.38 W. The MROA algorithm demonstrated superior performance, achieving an output power of 153.01 W, with a tracking accuracy of 99.11 % and a tracking duration of 5.2 s. In contrast, the ROA method attains 148.63 W with an accuracy of 96.28 % in 5.4 s, while the PSO method records 148.23 W with an accuracy of 96.02 % and a longer tracking time of 6.0 s. Figure 14 shows the tracking curves for the power, voltage, current, and duty cycle for all three methodologies. The MROA algorithm converged to the GMPP most rapidly and produced the highest power output, whereas the ROA and PSO methods exhibited slower response times.
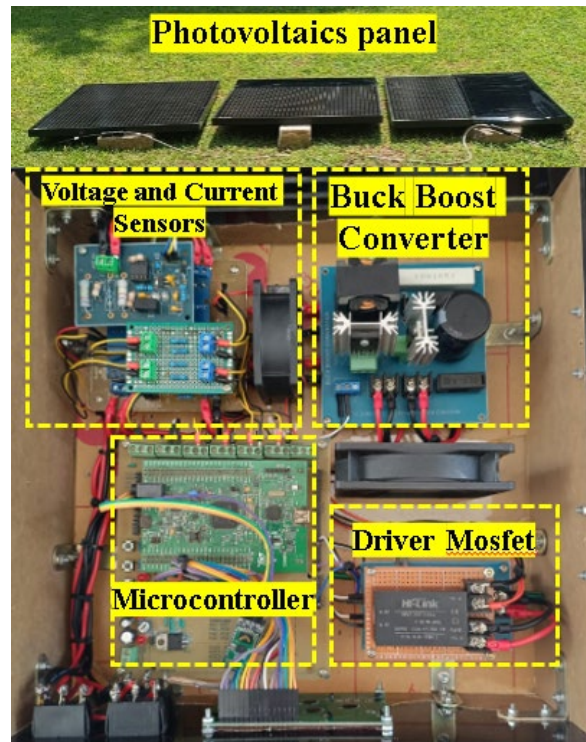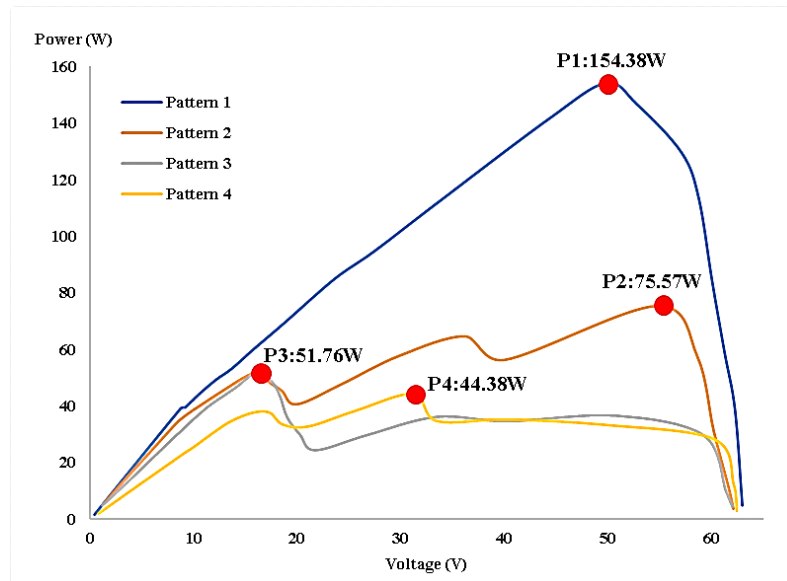

Figure 12. Experimental prototype.

Figure 13. P-V characteristics of the experimental test pattern.

The results obtained from Pattern 2 indicate that the MROA algorithm outperforms the other algorithms. Specifically, it tracks 75.04 W from a GMPP of 75.57 W with an accuracy of 99.30 % within a duration of 4.9 s. In contrast, the ROA algorithm achieves 73.74 W (97.58 %) in 5.4 s, whereas the PSO algorithm attains 74.81 W (98.99 %) but requires 6 s to do so. Figure 15 depicts the power tracking and control

signals, illustrating that the MROA delivers a more rapid and precise performance. Notably, the PSO algorithm results in the lowest output power, whereas the ROA algorithm requires a longer time to stabilize.

In Pattern 3, the Global Maximum Power Point (GMPP) is 51.76 W. The Modified ROA Algorithm (MROA) demonstrated superior performance, achieving an output of 51.65 W with an accuracy of
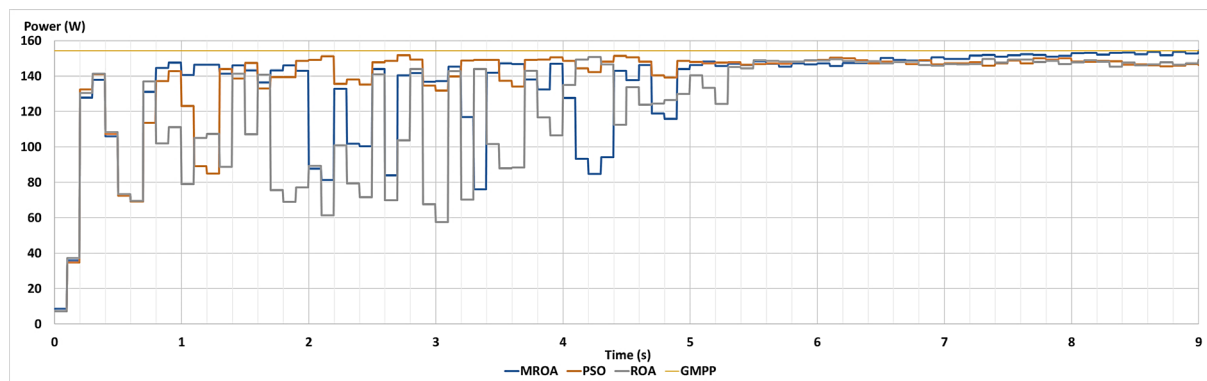

Figure 14. The experimental results of MROA, ROA, and the PSO algorithm pattern 1.
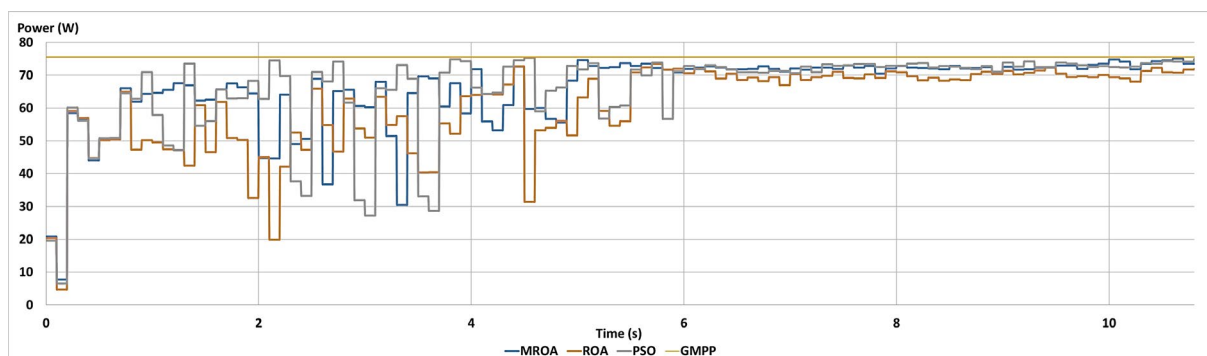

Figure 15. The experimental results of MROA, ROA, and the PSO algorithm pattern 2.
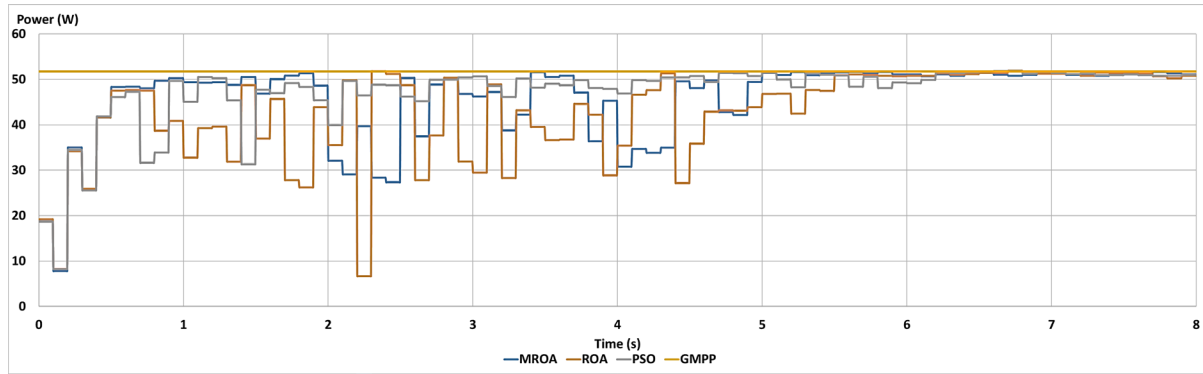
Figure 16. The experimental results of MROA, ROA, and the PSO algorithm pattern 3.
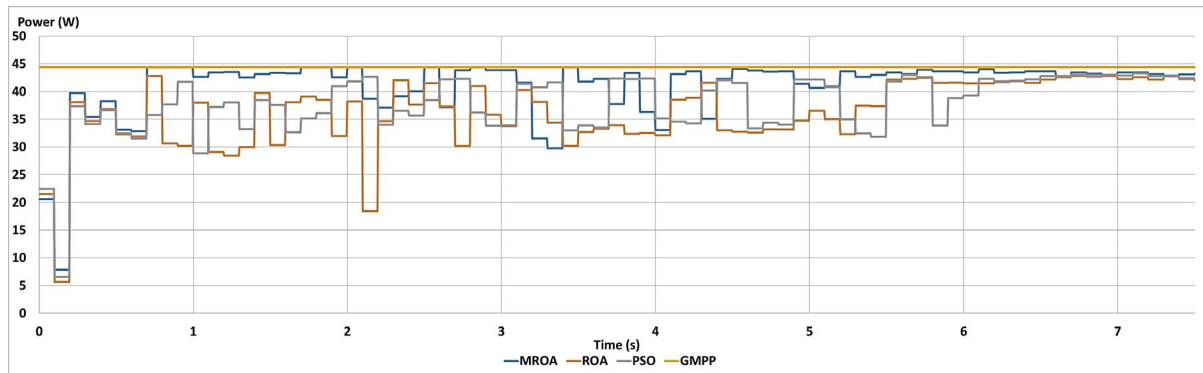

Figure 17. The experimental results of MROA, ROA, and the PSO algorithm pattern 4.

99.79 % and a tracking time of 5.1 s. The ROA Algorithm produces an output of 51.24 W with 99.00 % accuracy, while the particle swarm optimization (PSO) method performs slightly better, yielding 51.48 W with 99.46 % accuracy. However, both ROA and PSO require longer tracking times of 5.4 s and 6.0 s, respectively. Figure 16 shows the tracking waveforms of the power, voltage, current, and duty cycle. The MROA exhibits rapid convergence to the maximum power point, whereas the PSO tracks more slowly despite surpassing the ROA in the power output.

The results for Pattern 4 also highlight the dominance of the MROA. With a GMPP of 44.38 W, MROA approaches the maximum power with an output of 43.64 W, 98.33 % accuracy, and a tracking time of 5.4 s. ROA records a power of 42.69 W with 96.18 % accuracy with the same tracking time as ROA, namely 5.4 s, and PSO only produces 42.40 W with 95.54 % accuracy. PSO also requires the longest tracking time, at 6.0 s. Figure 17 shows the tracking results for Pattern 4. In this figure, it can be seen that MROA still achieves better power than the other methods, especially under lower power conditions. PSO exhibited a slower response and the lowest output among the three algorithms.

Figure 14 to Figure 17 illustrate the results of the hardware tests comparing the MROA, ROA, and PSO algorithms under the conditions of partial shading. Although all three algorithms are capable of identifying the global maximum power point (GMPP), they exhibit differences in terms of accuracy, speed, and stability. The PSO algorithm was the slowest and least stable, with an average tracking time of 6.0 s and an accuracy rate of 97.51 %. Under low-power conditions, it demonstrates significant power fluctuations after reaching the GMPP, thereby reducing energy capture. The ROA algorithm offers greater stability and faster tracking (5.4 s) with an accuracy of 97.26 %; however, it remains less effective under dynamic conditions. The MROA algorithm.

surpassed both, achieving the highest accuracy (99.13 %), fastest tracking time (5.15 s), and minimal power fluctuation. Owing to its high accuracy, rapid response, and stable power output, the MROA algorithm has emerged as the most effective and reliable maximum power point tracking (MPPT) method for enhancing photovoltaic system efficiency under varying shading conditions. Table 6 summarises the overall hardware-based tracking results.

Table 6.
Experimental test results data.

Pattern	Algorithm	GMPP (W)	Power output (W)	Accuracy (%)	Time tracking (s)
1	MROA	154.38	153.01	99.11	5.2
	ROA	154.38	148.63	96.28	5.4
	PSO	154.38	148.23	96.02	6.0
2	MROA	75.57	75.04	99.30	4.9
	ROA	75.57	73.74	97.58	5.4
	PSO	75.57	74.81	98.99	6.0
3	MROA	51.76	51.65	99.79	5.1
	ROA	51.76	51.24	99.00	5.4
	PSO	51.76	51.48	99.46	6.0
4	MROA	44.38	43.64	98.33	5.4
	ROA	44.38	42.69	96.19	5.4
	PSO	44.38	42.40	95.54	6.0

IV. Conclusion

The MROA algorithm has undergone comprehensive evaluation through both simulation and hardware implementation to address the challenges associated with solar panels under partial-shading conditions. During the tests, the MROA exhibited exceptional performance, achieving an average tracking accuracy of 99.13 % and an average tracking time of approximately 5.15 s. These results surpass the capabilities of ROA and PSO, providing more stable power with minimal oscillations once the global maximum power point (GMPP) is attained. The superiority of the algorithm over ROA and PSO was evident across all tested partial shadow patterns, consistently distinguishing global power peaks from local ones, even in low irradiation scenarios. The comparative analysis positions MROA as the leading MPPT algorithm. The MROA-MPPT algorithm demonstrates exceptional potential for next-generation photovoltaic systems due to its high tracking precision, rapid convergence, and robust stability, which are essential for efficient and intelligent energy management.

Acknowlegdements

Declarations

Author contribution

M.Z. Efendi, A. Adnaurrosyid, M.N. Habibi, R.P. Eviningsih, N.A. Windarko, and M.P. Jati contributed equally as the main contributors of this paper. All authors read and approved the final paper.

Funding statement

Competing interest

The authors declare that they have no known competing financial interests or personal relationships that could have appeared to influence the work reported in this paper.

Additional information

Reprints and permission: information is available at https://mev.brin.go.id/.

Publisher's Note: National Research and Innovation Agency (BRIN) remains neutral with regard to jurisdictional claims in published maps and institutional affiliations.

References

[1] B. K. Dora *et al.*, "The global electricity grid: A comprehensive review," *Energies*, vol. 18, no. 5, pp. 1152–1152, Feb. 2025.

[2] W. Wang, B. Yuan, Q. Sun, and R. Wennersten, "Application of energy storage in integrated energy

systems — A solution to fluctuation and uncertainty of renewable energy," *Journal of Energy Storage*, vol. 52, p. 104812, Aug. 2022.

[3] F. García-Lillo, E. Sánchez-García, B. Marco-Lajara, and P. Seva-Larrosa, "Renewable energies and sustainable development: A bibliometric overview," *Energies*, vol. 16, no. 3, p. 1211, Jan. 2023.

[4] N. Novas, R. M. Garcia, J. M. Camacho, and A. Alcayde, "Advances in solar energy towards efficient and sustainable energy," *Sustainability*, vol. 13, no. 11, p. 6295, Jun. 2021.

[5] O. A. Alimi, E. L. Meyer, and O. I. Olayiwola, "Solar photovoltaic modules' performance reliability and degradation analysis—A review," *Energies*, vol. 15, no. 16, p. 5964, Aug. 2022.

[6] Nikhil Kushwaha, Vinod Kumar Yadav, and R. Saha, "Effect of partial shading on photovoltaic systems performance and its mitigation techniques-a review," *Energy Sources, Part A: Recovery, Utilization, And Environmental Effects*, vol. 45, no. 4, pp. 11155–11180, Sep. 2023.

[7] M. A. M. Youssef, A. M. Mohamed, Y. A. Khalaf, and Y. S. Mohamed, "Investigation of small-scale photovoltaic systems for optimum performance under partial shading conditions," *Sustainability*, vol. 14, no. 6, p. 3681, Mar. 2022.

[8] C. Shao, A. Migan-Dubois, and D. Diallo, "Performance of PV array configurations under dynamic partial shadings," *EPJ Photovoltaics*, vol. 14, no. 21, p. 10, Jan. 2023.

[9] T. Alves, J. P. N. Torres, R. A. Marques Lameirinhas, and C. A. F. Fernandes, "Different techniques to mitigate partial shading in photovoltaic panels," *Energies*, vol. 14, no. 13, p. 3863, Jun. 2021.

[10] Y.-J. Chiu *et al.*, "Maximum power exploitation of photovoltaic system under fast-varying solar irradiation and local shading," *International Journal of Photoenergy*, vol. 2022, pp. 1–17, Aug. 2022.

[11] M. L. Katche, A. B. Makokha, S. O. Zachary, and M. S. Adaramola, "A comprehensive review of maximum power point tracking (MPPT) techniques used in solar PV systems," *Energies*, vol. 16, no. 5, p. 2206, Feb. 2023.

[12] N. Rouibah *et al.*, "Experimental assessment of perturb & observe, incremental conductance and hill climbing MPPTs for photovoltaic systems," *2020 2nd International Conference on Electronic Engineering and Renewable Energy Systems. (ICEERE). Lecture Notes in Electrical Engineering*, vol 681, pp. 461–467, Aug. 2020.

[13] M. A. Qureshi, F. Torelli, S. Musumeci, A. Reatti, A. Mazza, and G. Chicco, "A novel adaptive control approach for maximum power-point tracking in photovoltaic systems," *Energies*, vol. 16, no. 6, pp. 2782–2782, Mar. 2023.

[14] Y. Meng, Z. Chen, H. Cheng, E. Wang, and B. Tan, "An efficient variable step solar maximum power point tracking algorithm," *Energies*, vol. 16, no. 3, pp. 1299–1299, Jan. 2023.

[15] I. Owusu-Nyarko, M. A. Elgenedy, I. Abdelsalam, and K. H. Ahmed, "Modified variable step-size incremental

conductance MPPT technique for photovoltaic systems," *Electronics*, vol. 10, no. 19, p. 2331, Sep. 2021.

[16] M. Gopahanal Manjunath, C. Vyjayanthi, and C. N. Modi, "Adaptive step size based drift-free P&O algorithm with power optimiser and load protection for maximum power extraction from PV panels in stand-alone applications," *IET Renewable Power Generation*, vol. 15, no. 6, pp. 1270–1285, Feb. 2021.

[17] P. Verma *et al.*, "Meta-heuristic optimization techniques used for maximum power point tracking in solar PV system," *Electronics*, vol. 10, no. 19, p. 2419, Oct. 2021.

[18] M. Yaich, Youssef Dhieb, Mounir Bouzguenda, and Moez Ghariani, "Metaheuristic optimization algorithm of MPPT controller for PV system application," *E3S Web of Conferences*, vol. 336, pp. 00036–00036, Jan. 2022.

[19] A. M. Eltamaly, M. S. Al-Saud, and A. G. Abo-Khalil, "Performance improvement of PV Systems' maximum power point tracker based on a scanning PSO particle strategy," *Sustainability*, vol. 12, no. 3, p. 1185, Feb. 2020.

[20] A. Hassanat, K. Almohammadi, E. Alkafaween, E. Abunawas, A. Hammouri, and V. B. S. Prasath, "Choosing mutation and crossover ratios for genetic algorithms—A review with a new dynamic approach," *Information*, vol. 10, no. 12, p. 390, Dec. 2019.

[21] Fethi Khelaifa, Kheireddine Lamamra, and Djaafar Toumi, "Application of grey wolf optimization algorithm for maximum power point tracking of solar panels," *International Journal of Energetica*, vol. 9, no. 1, pp. 17–17, Aug. 2024.

[22] S. Krishnan G, S. Kinattingal, S. P. Simon, and P. S. R. Nayak, "MPPT in PV systems using ant colony optimisation with dwindling population," *IET Renewable Power Generation*, vol. 14, no. 7, pp. 1105–1112, Mar. 2020.

[23] Samia Dziri, Soufiene Bouallègue, M. M. Alhato, and P. Siarry, "Artificial bee colony optimization–based enhancement of output power generation in grid-connected photovoltaic systems," *Transactions of the Institute of Measurement and Control*, Jan. 2025.

[24] N. Douifi, Amel Abbadi, Fethia Hamidia, K. Yahya, M. Mohamed, and N. Rai, "A novel MPPT based reptile search algorithm for photovoltaic system under various conditions," *Applied Sciences*, vol. 13, no. 8, pp. 4866–4866, Apr. 2023.

[25] M. Alshareef, "An effective falcon optimization algorithm based MPPT under partial shaded photovoltaic systems," *IEEE Access*, pp. 1–1, 2022.

[26] A. Sharma, Vibhu Jately, M. Averbukh, S. Rajput, and B. Azzopardi, "A novel TSA-PSO based hybrid algorithm for GMPP tracking under partial shading conditions," *Energies*, vol. 15, no. 9, pp. 3164–3164, Apr. 2022.

[27] H. Jia, X. Peng, and C. Lang, "Remora optimization algorithm," *Expert Systems with Applications*, vol. 185, p. 115665, Dec. 2021.

[28] R. A. Marques Lameirinhas, J. P. N. Torres, and J. P. de Melo Cunha, "A photovoltaic technology review: History, fundamentals and applications," *Energies*, vol. 15, no. 5, p. 1823, Mar. 2022.

[29] J. Teo, R. Tan, V. Mok, V. Ramachandaramurthy, and C. Tan, "Impact of partial shading on the P-V characteristics and the maximum power of a photovoltaic string," *Energies*, vol. 11, no. 7, p. 1860, Jul. 2018.

[30] V. Jha, "Mathematical modelling of PV array under partial shading condition," *Sādhanā*, vol. 47, no. 2, Apr. 2022.

[31] E. Molina-Santana, F. Gonzalez-Montañez, J. U. Liceaga-Castro, V. M. Jimenez-Mondragon, and I. Siller-Alcala, "Modeling and control of a DC-DC buck–boost converter with non-linear power inductor operating in saturation region considering electrical losses," *Mathematics*, vol. 11, no. 22, p. 4617, Nov. 2023.

[32] A. Alanazi, M. Alanazi, S. Arabi, and S. Sarker, "A new maximum power point tracking framework for photovoltaic energy systems based on remora optimization algorithm in partial shading conditions," *Applied Sciences*, vol. 12, no. 8, p. 3828, Apr. 2022.

[33] R. Zheng *et al.*, "An improved remora optimization algorithm with autonomous foraging mechanism for global optimization problems," *Mathematical Biosciences and Engineering*, vol. 19, no. 4, pp. 3994–4037, Jan. 2022.